Materials Today Bio 28 (2024) 101248

Contents lists available at ScienceDirect

Materials Today Bio

journal homepage: www.journals.elsevier.com/materials-today-bio

A Janus hydrogel that enables wet tissue adhesion and resists abdominal adhesions

Hanjie Shao [a,1], Junjie Deng [b,c,d,1], Zeping Xu [a,1], Jiujun Zhu [e], Wei Jian [f], Peiru Zhang [g], Xinhua Zhou [a], Xie Zhang [a], Hao She [a], Jingyun Ma [a,**], Xiang Wu [a,***], Hong Li [a,*]

[a] Ningbo Medical Center Li Huili Hospital, Health Science Center, Ningbo University, Ningbo, 315000, PR China
[b] Institute of Biomedical Engineering, Ningbo Institute of Materials Technology and Engineering, Chinese Academy of Sciences, Ningbo, 315201, PR China
[c] Zhejiang International Scientific and Technological Cooperative Base of Biomedical Materials and Technology, Ningbo Cixi Institute of Biomedical Engineering, Ningbo, 315300, PR China
[d] Wenzhou Medical University, Wenzhou, 325035, PR China
[e] Department of Microelectronics, School of Physical Science and Technology, Ningbo University, PR China
[f] School of Mechanical Engineering & Mechanics, Ningbo University, Ningbo, 315211, PR China
[g] The Fourth School of Clinical Medicine, Zhejiang Chinese Medical University, Hangzhou, 310053, PR China

ARTICLE INFO

Keywords:
Hydrogel
Wet adhesion
Janus
Rapid hemostasis
Anti-adhesion

ABSTRACT

Hydrogels have indeed achieved significant advancements, yet their clinical translation has been hampered by their inherent limitations in wet adhesion properties. Furthermore, the design of adhesive hydrogels that can resist postoperative adhesions remains an intricate challenge. In this study, we introduce a Janus hydrogel (JGP) that offers a novel approach to address these challenges. The JGP hydrogel has two asymmetrical sides, consisting of an adhesion layer (AL) and an anti-adhesion layer (AAL). Specifically, the AL incorporates three key components: N-[tris(hydroxymethyl)methyl]acrylamide (THMA), acrylic acid (AAc), and the acrylic acid N-hydroxysuccinimide ester (AAc-NHS). By drying the AL, it has a rapid water absorption capability. The abundance of hydroxyl and carboxyl groups in the AL enables the formation of robust hydrogen bonds with tissues, thereby achieving superior adhesive properties. Additionally, the synergistic effect of THMA's tridentate hydrogen bonding and the covalent bonding formed by AAc-NHS with tissue ensures long-lasting wet adhesion. To realize the anti-adhesion function, one side of the AL was immersed in a solution of [2-(methacryloyloxy) ethyl]dimethyl-(3-sulfopropyl)ammonium hydroxide (SBMA), which undergoes crosslinking to form the AAL. A comprehensive series of tests have confirmed that the JGP hydrogel exhibits exceptional mechanical properties, efficient and enduring adhesion, excellent biocompatibility, and degradability. Moreover, it possesses remarkable hemostatic properties and robust anti-abdominal adhesion characteristics.

1. Introduction

Hydrogels are widely used in the field of tissue engineering due to their excellent three-dimensional mesh structure and high-water content [1–3]. Among them, adhesive hydrogels have developed particularly rapidly and have been used in several fields of medical treatment, such as applications in wound closure as well as drug release [4–6]. However, unfortunately, the adhesive hydrogels (e.g., cyanoacrylates and fibrin glue) used in clinical practice nowadays are limited in their ability to bond to wet tissues, which greatly hinders the application and development of hydrogels [1]. In addition, the poor biocompatibility of cyanoacrylate-based adhesives greatly limits their development [6,7]. The hydration layer on the wet tissue surface is the main reason for the limited adhesion, which prevents the hydrogel-wet tissue interface from interacting [8–10]. Hydrogels with good wet tissue adhesion appear to be particularly important in many aspects, such as applications in hemorrhage, gastric perforation, and pneumothorax [11–15]. Adhesive hydrogels have better biocompatibility and ease of handling compared

* Corresponding author.
** Corresponding author.
*** Corresponding author.
E-mail addresses: majingyun198401@126.com (J. Ma), 2111101032@nbu.edu.cn (X. Wu), lihong196311@163.com (H. Li).
[1] H. Shao, J. Deng and Z. Xu contributed equally to this work.

https://doi.org/10.1016/j.mtbio.2024.101248
Received 15 July 2024; Received in revised form 26 August 2024; Accepted 13 September 2024
Available online 14 September 2024

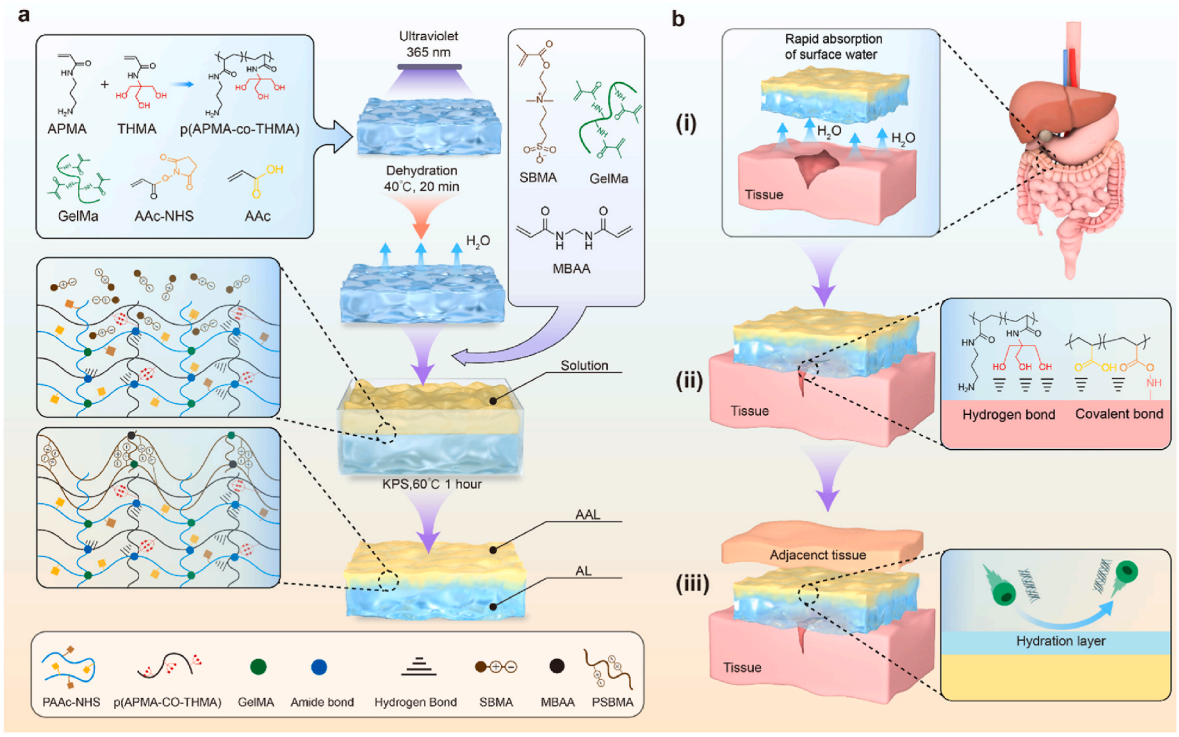

Fig. 1. JGP design as well as mechanism. (a) JGP preparation process. It mainly includes photocrosslinking, dewatering, one-sided immersion, and thermal crosslinking. (b) Schematic representation of the mechanism of wet tissue adhesion as well as resistance to abdominal adhesion. (i) JGP exhibits the ability to rapidly absorb water. (ii) Multiple adhesion mechanisms, including tridentate hydrogen bonding, hydrogen bonding of carboxyl groups and covalent amide bonding, which together achieve rapid and durable wet tissue adhesion. (iii) JGP forms a hydration layer on its surface in the presence of SBMA thereby achieving anti-postoperative adhesions.

to U-shaped staples and surgical sutures [16].

Inspired by natural organisms, scientists have discovered that the effect of underwater adhesion in mussels is caused by mussel foot proteins (Mfps) [17,18]. The 3,4-dihydroxyphenylalanine (DOPA) in Mfps plays important functions in wet tissue adhesion, including DOPA-mediated hydrophobicity and dentate hydrogen bonding [19]. Indeed, the catechol structure in DOPA is susceptible to oxidation, but the reducing group in Mfps solves this problem [20]. Inspired by DOPA, numerous scientists have investigated a variety of tissue patches that can achieve underwater adhesion with a catechol moiety (catechol) as the core [21]. For example, North et al. used poly (catechol-styrene) to mimic the adhesion effect of Mfps. The experimental results showed the excellent underwater adhesion effect of this material [22]. Fu et al. prepared a highly biocompatible gel using carboxymethyl cellulose grafted with dopamine and acrylamide grafted with dopamine. It exhibited underwater adhesion properties up to 86.3 ± 7.2 kPa. Unfortunately, the catechol moiety causes a decrease in adhesion due to oxidation, so the sustained adhesion performance is yet to be demonstrated [7,23,24]. Li et al. achieved antioxidant effects through the synergistic effect of tannins and Mfp6 mimetic protein (polyglutamic acid-Cys) [25]. Zhang et al. prepared injectable Janus gels by utilizing the mechanism that catechol are susceptible to oxidation and lead to a decrease in adhesion [26]. Thus, mimicking the adhesion mechanism of mussels requires a tightly controlled redox environment, but this is usually more complex and time-consuming.

Furthermore, prevention of postoperative surgical adhesions is one of the major clinical challenges [7,27]. Postoperative abdominal adhesions occur in 80 % of patients undergoing abdominal surgery [28]. Abdominal adhesions can lead to serious complications such as intestinal obstruction [29]. Therefore, there is an urgent need for an asymmetric double-sided tissue patch with both durable and high-strength adhesive properties and resistance to abdominal adhesions.

To fulfill these two properties, an asymmetric adhesion/anti-adhesion Janus hydrogel patch (JGP) was designed in this study. In the adhesion layer (AL), we introduced a substance with "three-tooth hydrogen bonding". This substance (p(ATMA-co-THMA)) is formed by the copolymerization of N-[tris(hydroxymethyl)methyl]acrylamide (THMA) with N- (3-aminopropyl)methacrylamide hydrochloride (APMA). P(ATMA-co-THMA) has a high density of hydrogen bonds and has a strong adhesive effect on tissues [30]. The adhesion layer was mainly composed of acrylic acid (AAc), acrylic acid N-hydroxysuccinimide ester (AAc-NHS), p(ATMA-co-THMA), and biodegradable methacrylic anhydride gelatin (GelMA) [31,32]. Considering the dynamic and humid environment in the abdominal cavity, the removal of surface water and layers of tissue adhesion is crucial for wet adhesion. For this purpose, drying of the AL was performed to provide the AL with the ability to absorb water quickly. The formation of strong adhesion between the AL and the tissue relies mainly on the hydrogen bonding from the carboxyl and hydroxyl groups as well as the covalent bonding formed by the NHS groups with the tissue (Fig. 1b (i)-(ii)). For the anti-adhesion layer (AAL), [2-(methacryloyloxy)ethyl]dimethyl-(3-sulphonatopropyl)ammonium hydroxide (SBMA) was introduced by one-sided immersion and thermally crosslinked to form an asymmetric Janus hydrogel, which is called JGP. SBMA forms a hydration layer on the surface due to its good hydrophilicity. It prevents the formation of hydrogen or covalent bonds between the hydrogel and the tissue surface, thus preventing adhesion. At the same time the hydration layer is resistant to cell and protein adhesion and prevents the formation of tissue adhesions (Fig. 1b (iii)). [31,33]. The analysis in this study assessed the adhesion properties of the patches by lap-shear experiments, burst pressure test, and underwater adhesion experiments; the mechanical properties of the patches by compression and tensile tests; and the degradability and biocompatibility of the patches by hemolysis, CCK-8, live/dead staining experiments, and subcutaneous degradation experiments. Finally, the hemostatic properties were assessed by a liver bleeding model; and the anti-adhesion properties of the patches were

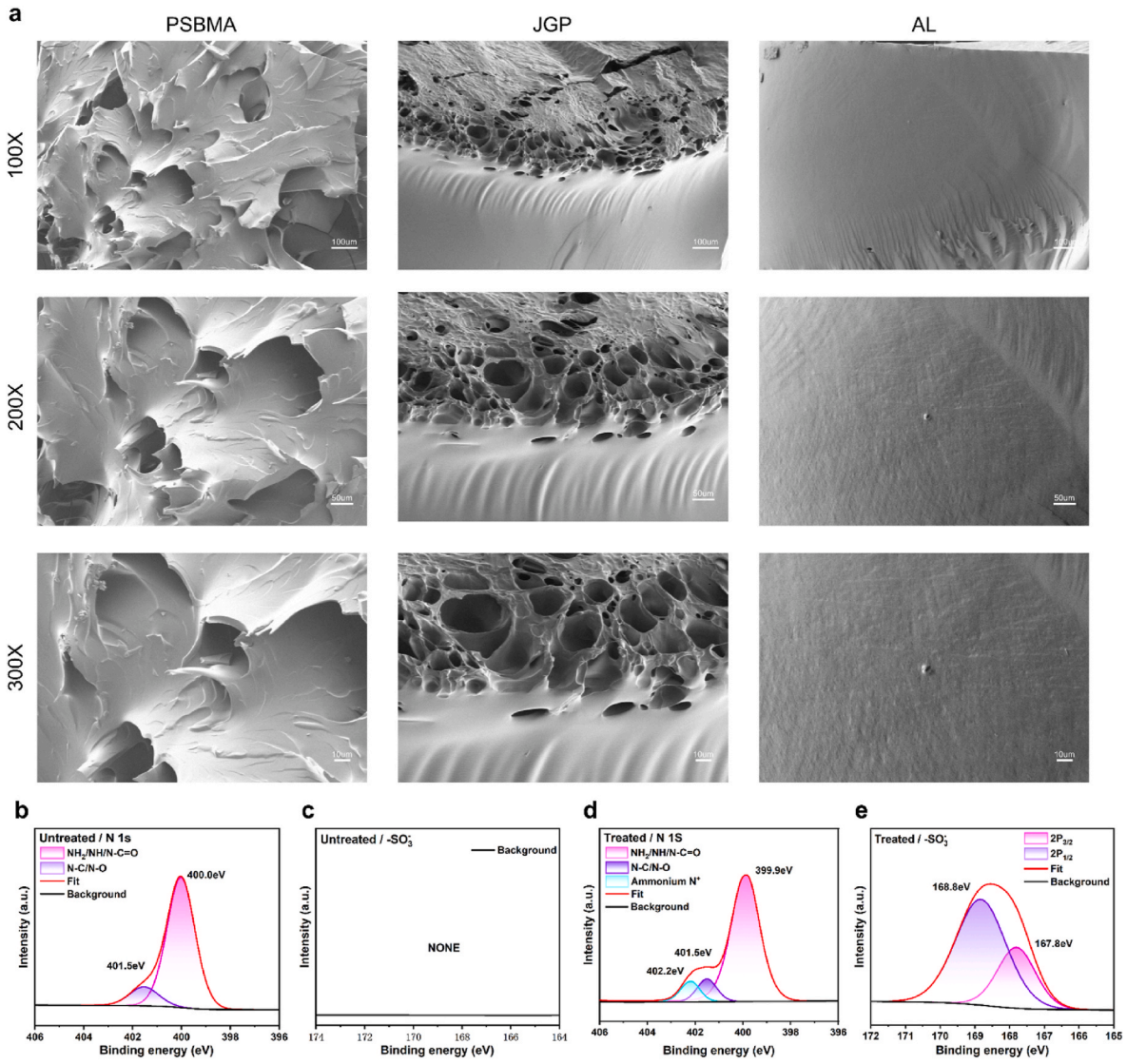

Fig. 2. Differences before and after immersion. (a) SEM images of PSBMA, JGP transition layer, and AL. (b) XPS high-resolution spectra of N 1s and S 2p of hydrogels before and after one-sided immersion with SBMA solution.

assessed by a cecum injury model.

2. Materials and methods

2.1. Materials

Acrylic acid (AAc, >99 %), acrylic acid N-hydroxysuccinimide ester (AAc-NHS, >98 %), lithium phenyl-2,4,6-trimethylbenzoyl hypophosphite (LAP, >98 %), photoinitiator, N-(3-aminopropyl)methacrylamide hydrochloride (APMA, >98 %), N-[tris(hydroxymethyl) methyl]acrylamide (THMA. 93 %), gelatin, methacrylic anhydride (94 %), [2-(methacryloyloxy)ethyl]dimethyl-(3-sulphonatopropyl)ammonium hydroxide (SBMA, >97 %) from Aladdin Biochemistry Science and Technology Co (China). Ammonium persulfate (APS, 99.99 %), and N, N′-methylenebisacrylamide (MBAA, 99 %) were provided by Shanghai Macklin Biochemical Corporation (China). All chemicals were of analytical grade as required and could be used without further purification.

2.2. Synthesis of p(APMA-co-THMA) and GelMA

P(APMA-co-THMA) was synthesized by free radical polymerization with some modifications in reference to the method of Chen et al. [34] (Fig. S1). First, THMA (728 mg) and APMA (185 mg) were dissolved in 6 mL of deionized water in a nitrogen atmosphere. Then APS (23 mg) was added to initiate the polymerization at 60 °C. After 1 h, the temperature was adjusted to 70 °C, and the reaction was terminated after 7 h. At the end of the reaction, it was dialyzed in deionized water (molecular weight cut-off of 3500D-7000D). Dialysis was performed for at least three days with at least three water changes per day. After dialysis, p(APMA-co-THMA) was obtained by freeze-drying. The obtained p (APMA-co-THMA) was sealed and stored at −20 °C until further use.

The synthesis of GelMA was obtained by following the previous method with some modifications [35]. Briefly, 10 g was dissolved in 100 mL of phosphate buffer solution (PBS) and after complete dissolution at 60 °C, 6 mL of methacrylic anhydride was added slowly and homogeneously dropwise to the solution. The temperature was then adjusted to 50 °C and the reaction was carried out for 1 h. After finishing the reaction, the solution was dialyzed in deionized water (molecular weight cut-off of 8KD-14KD). Dialyze for at least three days with at least three water changes per day. After dialysis, GelMA was freeze-dried and the obtained GelMA was sealed and stored at −20 °C until further use.

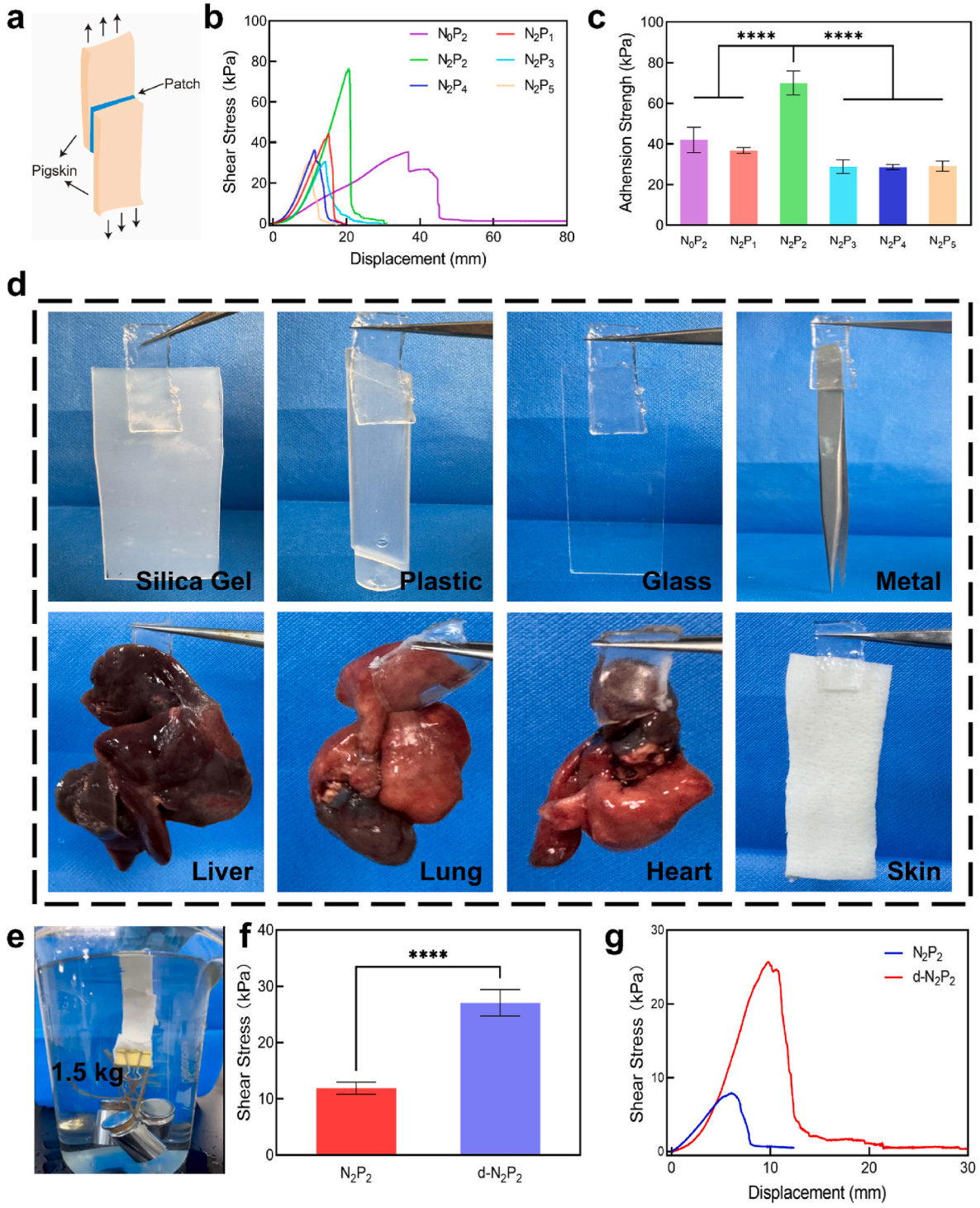

Fig. 3. Adhesion properties of N_XP_Y. (a) Schematic diagram of lap shear. (b) Stress-displacement graphs of lap-shear tests of different concentrations of N_XP_Y with dry pork skin. (c) Histogram of maximum stress of lap shear test of different concentrations of N_XP_Y with dry pig skin. (d) Adhesion diagrams of AL with various tissues and various materials. (e) Underwater, AL can lift a weight of about 1.5 kg. (f) Stress-displacement graphs of lap-shear tests of undried N_2P_2 and dried d-N_2P_2 with wet pigskin. (g) Histograms of maximum stresses for lap shear tests of undried N_2P_2 and dried d-N_2P_2 against wet pigskin.

2.3. Characterization of synthesized materials

The structures of p(APMA-co-THMA) and GelMA were verified by ^{1}H nuclear magnetic resonance (^{1}H NMR) spectroscopy (Ascend 400 MHz Brukerz, D_2O).

2.4. Synthesis of JGP

The preparation process of JGP is shown in Fig. 1a. For AL, an amount of p(APMA-co-THMA), 0.02 g of GelMA, and 0.02 g of LAP were first added to 10 g of water. After being fully dissolved and stirred well at 40 °C, 3 g of AAc and an amount of AAc-NHS were added, followed by stirring well. For convenience of description, AAc-NHS is named N_XP_Y when it is X% of the water mass and p(APMA-co-THMA) is Y% of the

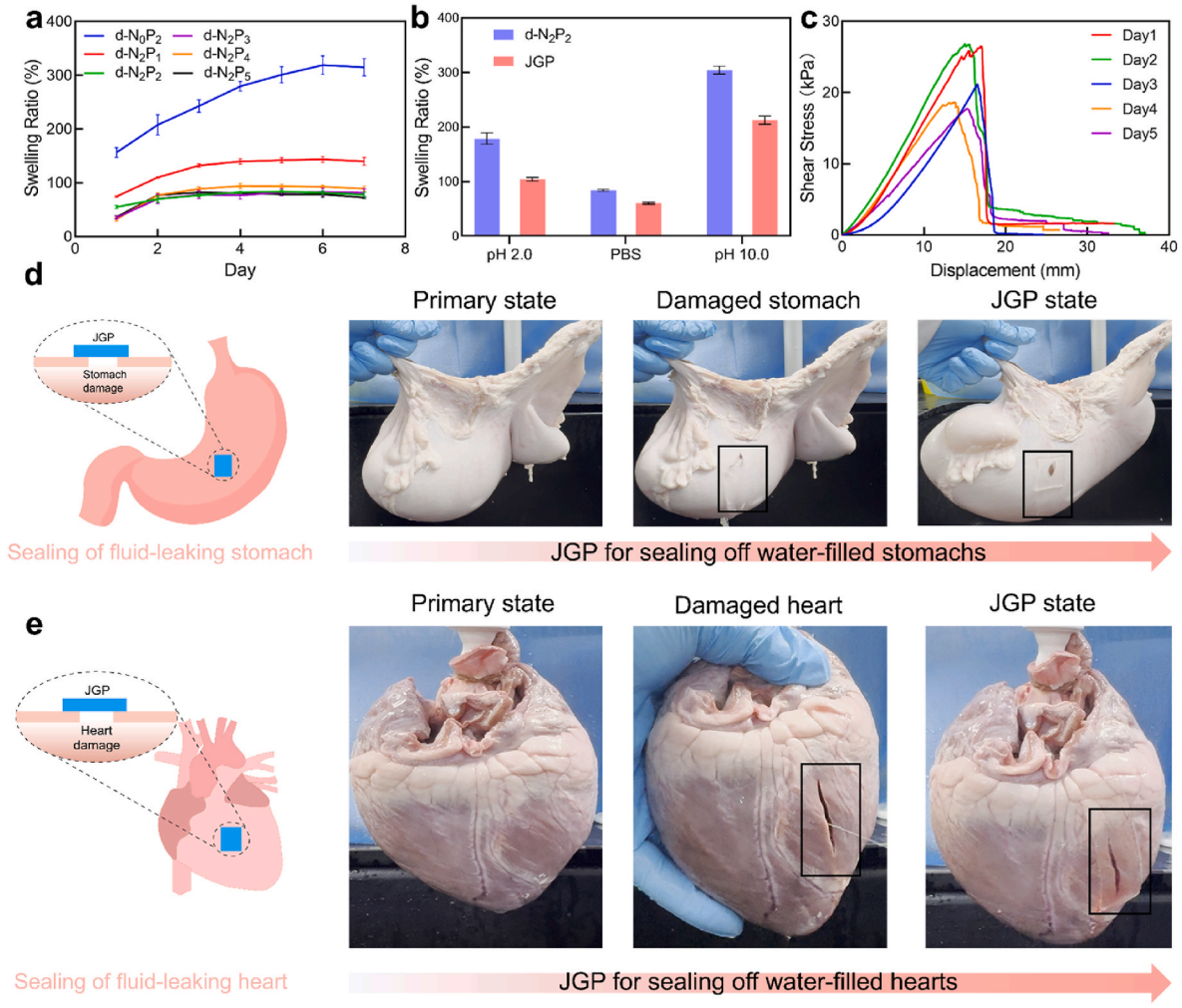

Fig. 4. Swelling and adhesion properties. (a) Swelling curves of different concentration components. (b) Comparison of the swelling rates of JGP and d-N_2P_2. (c) Changes in the adhesion of d-N_2P_2 for different swelling times. (d) Liquid sealing properties of hydrogels on ruptured porcine stomachs. (e) Liquid sealing properties of hydrogels on ruptured pig hearts.

water mass. The specific content is detailed in the Supporting Information Table S1. Nitrogen was passed into the mixture to remove oxygen. Under the nitrogen atmosphere, the mixture was injected into a glass plate mold and crosslinked under UV light at a wavelength of 365 nm for 30 min to form a gel. Subsequently, the adhesive layer was first soaked in deionized water to remove the biotoxic monomer molecules, followed by drying at 40 °C for 20 min. The d-N_XP_Y (AL) was obtained.

For AAL, 2 g of SBMA, 0.2 g of GelMA, 0.06 g of MBAA, and 0.1 g of APS were firstly added to 10 g of water and then the mixed solution was stirred well. The dried AL was placed in a mold and immersed in the solution for 30 min on one side, and then the immersed AL was placed in the mold and thermally crosslinked for 60 min at 60 °C. The resulting product is noted as JGP. For ease of description, unless otherwise specified, JGP is obtained by crosslinking by immersion in N_2P_2.

2.5. Characterization of microstructure

To evaluate the microstructures of PSBMA gel, JGP transition layer, and AL, the freshly prepared PSBMA gel, JGP, and AL were frozen in a refrigerator at −80 °C for 8 h, and then freeze-dried to obtain dried samples. The microstructure of JGP was observed by scanning electron microscopy (SEM, TM-3000, HITACHI).

2.6. Surface chemical composition of JGP

Changes in the chemical composition of the hydrogel surface before and after SBMA immersion were observed by X-ray photoelectron spectroscopy (XPS, K-Alpha, Thermo Fisher Science).

2.7. Evaluation of swelling behavior

To evaluate the swelling behavior of the different components of AL and JGP, patches of a certain size were immersed in phosphate-buffered saline (PBS, pH = 7.4), pH 2 and pH 10 at 37 °C and shaken at 60 rpm. At each specific time point, the surface was wiped off and the patches were then weighed. The swelling ratio was calculated using the following formula:

$$\text{Swelling ratio}\ (\%) = (W_t - W_0)\ /\ W_0$$

Where W_0 is the weight of the freshly prepared hydrogel patch on day 0 and W_t is the weight of the dissolved hydrogel patch on day t. All tests were repeated 4 times for each group.

2.8. Evaluation of tissue adhesive and sealing properties

To determine the adhesion properties of AL, lap-shear experiments were performed. Pigskin was sheared 25 mm × 75 mm, and AL was

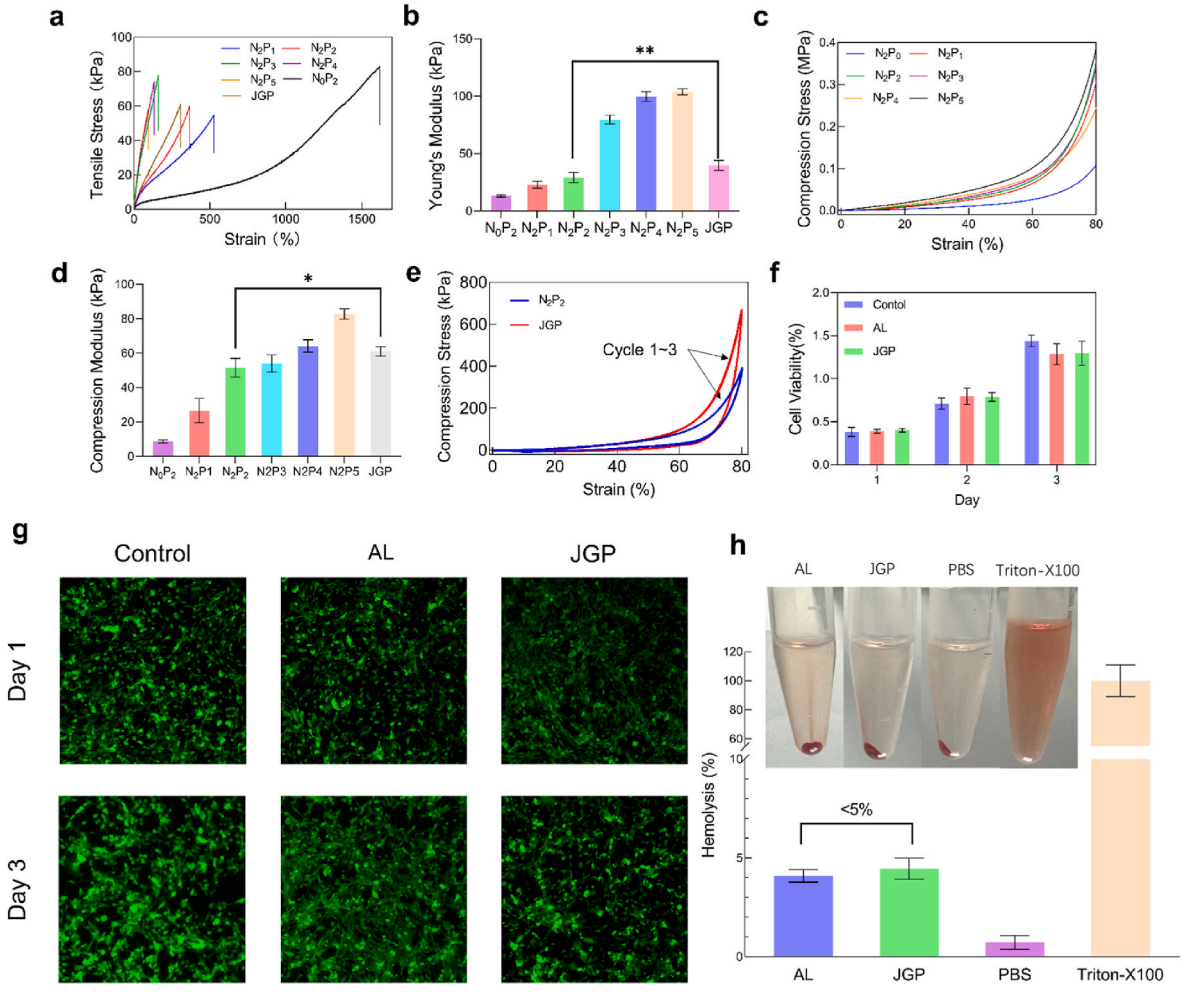

Fig. 5. (a) Tensile strain-stress plots for groups with different concentrations. (b) Comparison of Young's modulus for groups with different concentrations. (c) Compressive strain-stress plots for groups of different concentrations. (d) Compression modulus comparison of groups with different concentrations. (e) Compression cyclic strain-stress diagrams for N_2P_2 and JGP (3 cycles). (f) The viability of L929 cells after AL and JGP treatments was tested by CCK-8. (g) Live/dead staining of L929 cells treated with AL and JGP. (h) Results of hemolysis experiments with AL and JGP.

bonded to two pieces of pigskin with an overlap size of 25 mm × 30 mm. A soft matter mechanical tester (INSTRON) equipped with a 1000 N mechanical transducer was used, and two pieces of pigskin were clamped at each end of the tester's fixture at a constant displacement rate of 20 mm/min. The lap shear strength was calculated as follows:

$$\text{Lap} - \text{stress} = F_{Max} / (W \times l)$$

where F_{Max} is the maximum force during lap shear and W, l are the width and length of the AL, which are fixed constants.

For the wet tissue adhesion properties of AL, the AL was adhered to two pieces of pigskin after the surface of the two pieces was wetted with a certain amount of liquid. The two pieces of pigskin were clamped at each end of the fixture of the testing machine at a constant displacement rate of 20 mm/min. The lap shear strength was calculated as described above.

To determine the sealing ability of the JGP, the JGP was subjected to a liquid tightness test and a gas tightness test. For liquid tightness, a certain size of wound was cut on the water-filled pig heart and stomach, and then the JGP was attached to observe the sealing. And we conducted a burst pressure test in order to quantify the sealing. We built our own model, which is shown schematically in Fig. S6. The pig skin damage was about 1 cm and the hydrogel size was about 3 cm × 3 cm. Nitrogen was filled and the pressure at the time of bursting was recorded.

2.9. Evaluation of mechanical property

To evaluate the mechanical properties of different fractions of AL and JGP, they were tested in tensile test, compression test. Any test was repeated 3 times for each sample. For the tensile test, a soft matter mechanical testing machine (INSTRON) equipped with a 10 N mechanical transducer was used. For the tensile tests, the patches were tested in a dumbbell shape at a constant displacement rate of 20 mm/min. The length, width, and thickness of AL and JGP were 75 mm × 4 mm × 2 mm and 75 mm × 4 mm × 2 mm, respectively, For the compression experiments, a soft-matter mechanical tester equipped with a 1000 N mechanical transducer (INSTRON) was used. In the compression test, the sample was tested in the shape of a cylinder and at a constant displacement rate of 20 mm/min. The test ends when the strain reaches 80 %. To test the fatigue resistance of the material, a compression-unloading cycle with three repetitions was performed.

2.10. In vitro and In vivo biocompatibility and antimicrobial testing

Both JGP and AL (d-N_2P_2) were sterilized by UV irradiation before being used in the following series of biocompatibility tests. The in vitro experiments were CCK-8 assay, Live/Dead staining, and hemolysis assay. The *in vivo* experiments were subcutaneous degradation experiments. To evaluate the in vitro cytocompatibility of JGP and AL (d-N_2P_2), JGP and AL (d-N_2P_2) were immersed in culture medium at 37 °C

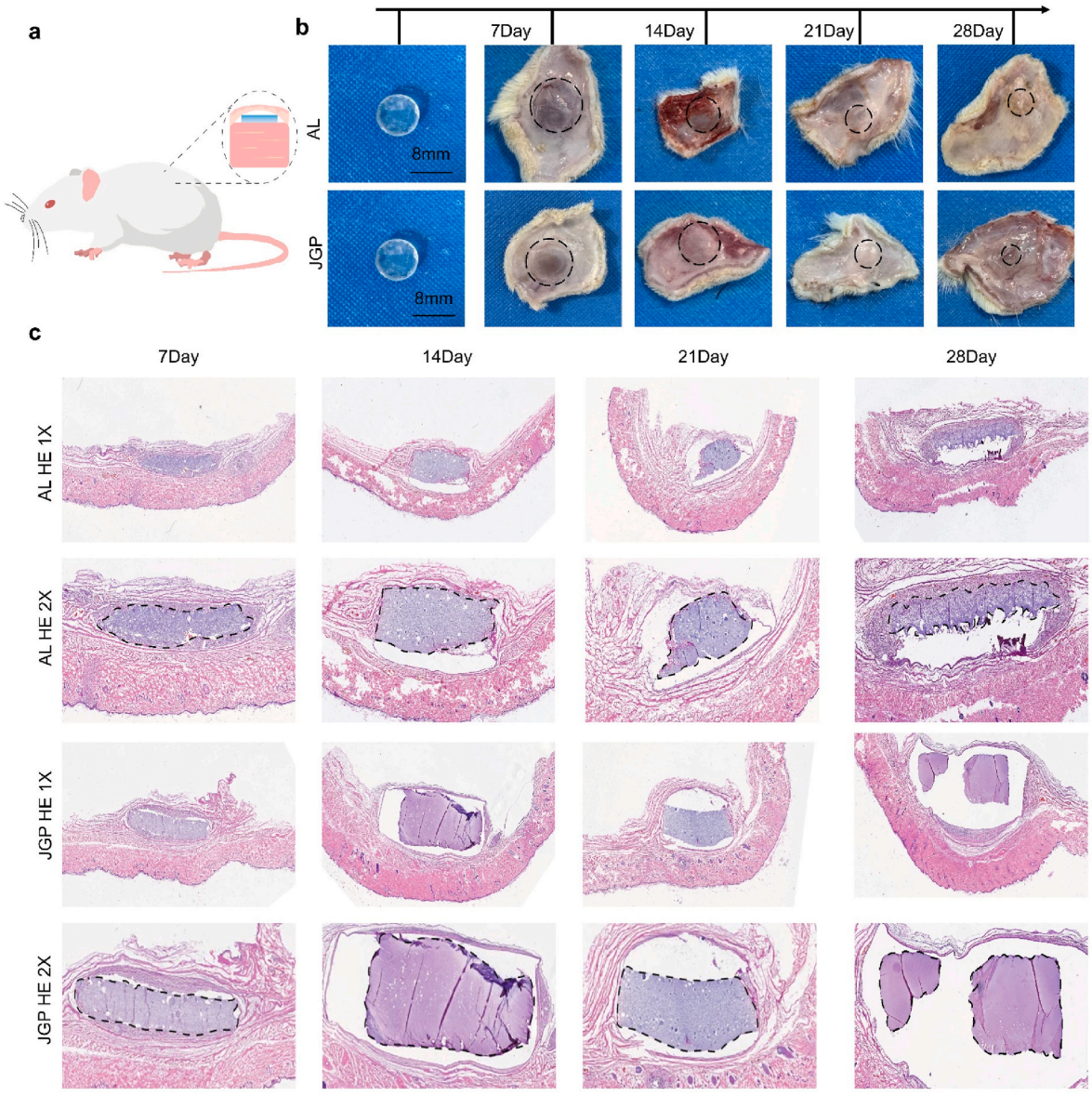

Fig. 6. (a) Schematic diagram of subcutaneous degradation model. (b) Photographs of JAP and AL at 0, 1, 2, 3, and 4 weeks after implantation. (c) HE-stained images of subcutaneously implanted JGP and AL at 1, 2, 3, and 4 weeks. The upper side of the patch is AAL and the lower side is AL.

for 24h to prepare JGP medium and AL (d-N_2P_2) medium. L929 cells were treated with JGP medium, AL (d-N_2P_2) medium, and the original medium and incubated with the cells.

For the CCK-8 assay, L929 cells were incubated in a CO2 incubator at 37 °C for 1,2,3 days. Cell activity was analyzed at a fixed time point within 3 days using a microplate reader.

For Live/Dead staining, similar to the CCK-8 assay, cells were incubated with live/dead dye at a specific time point on day 1,3 of incubation, and then live/dead stained images were captured under a confocal microscope.

For hemolysis experiments, hydrogel extracts were prepared beforehand by placing 100 mg of JGP and AL (d-N_2P_2) in 1 mL of PBS (10 ×), respectively, at 37 °C after 24h. 1 mL of rat blood was collected in EDTA anticoagulation tubes and centrifuged in a centrifuge at 2000 rpm and 4 °C for 10 min, and the supernatant was discarded. It was washed four times with 0.9 % saline and a 2 % erythrocyte suspension was prepared with PBS. The erythrocyte suspension and the extracts of JGP and AL (d-N_2P_2) were mixed in the ratio of 9:1. PBS was used as a negative control and 1 % concentration of Triton X-100 was used as a positive control. Then it was placed in constant temperature at 37 °C for 2 h. After the incubation was completed, the extracts were centrifuged at 2000 rpm and 4 °C for 10 min, and the supernatants (100 μL) of the control and experimental groups were taken in a 96-well plate, respectively, and the absorbance (OD) at 541 nm was measured at 541 nm for each group using an enzyme labeler. The hemolysis rate was calculated according to the following formula:

$$\text{Hemolysis}\ (\%) = (OD_{Sa} - OD_{Ne}) \ / \ (OD_{Po} - OD_{Ne})$$

Where OD_{Sa} is the OD value of JGP and N2P2 groups, OD_{Ne} is the OD value of the negative control group, and OD_{Po} is the OD value of the positive control group.

All animal experiments complied with the permission of the Laboratory Animal Welfare and Ethics Committee of Ningbo University (NBU20240296). To evaluate the *in vivo* biocompatibility of JGP and AL (d-N_2P_2), JGP-based and AL (d-N_2P_2)-based were implanted into the dorsal subcutaneous tissues of Sprague-Dawley (SD) rats (male, 8 weeks, 220 g–250 g). SD rats were anesthetized by intraperitoneal injection of sodium pentobarbital. The dorsal skin was excised and disinfected on

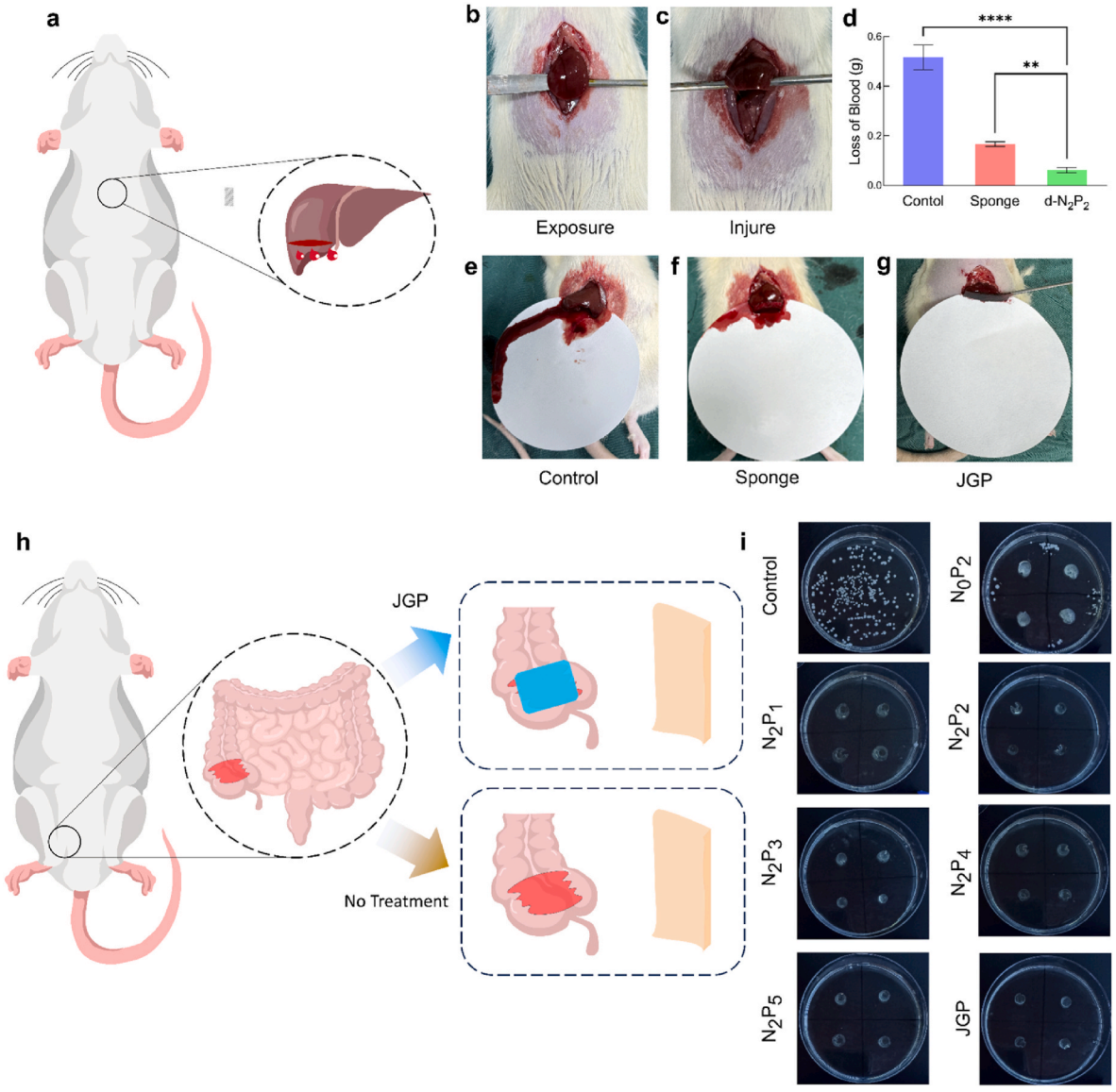

Fig. 7. (a): (i)Schematic diagram of the liver hemorrhage model. (ii) Schematic diagram of the cecum injury model. (b) Liver exposure. (c) Liver injured. (d) Comparison of bleeding in different groups. (e) Bleeding photographs of the control group. (f) Bleeding photographs of the sponge group. (g) Bleeding photographs of the JGP group. (h) Antimicrobial effect of different groups against *Staphylococcus aureus*.

the surface. Penicillin was given postoperatively to prevent postoperative infection. The rats were executed and the tissues on the back were taken out at the first, second, third, and fourth weeks after implantation. To observe the explanation of JGP and d-N_2P_2, the tissues were photographed and HE stained.

For the antimicrobial experiments, the *S. aureus* bacterial solution was spread evenly and flatly over the entire surface of the petri dish, and the cylindrical N_XP_Y (6 mm × 6 mm) was placed on top of the petri dish, and then incubated at 37 °C for 24 h to observe the results.

2.11. *In vivo hemostasis test and anti-abdominal adhesion test*

All animal experiments complied with the permission of the Laboratory Animal Welfare and Ethics Committee of Ningbo University (NBU20240296). To evaluate the *in vivo* hemostatic effect of JGP, a liver injury model was used. SD rats (male, 8 weeks, 220 g–250 g) were anesthetized by intraperitoneal injection of sodium pentobarbital. The abdomen was removed and the surface of the abdomen was sterilized. The skin on the upper side of the abdomen was incised to expose the liver. Filter paper (weighed in advance) was placed underneath the liver and a wound of a certain size was made in the liver. The wound was then treated with three subgroups, JGP, gelatin sponge, and no treatment. After waiting for 3 min, the filter paper was removed and weighed. The mass obtained minus the original weight is the amount of bleeding. Each group was tested four times.

All animal experiments complied with the permission of the Laboratory Animal Welfare and Ethics Committee of Ningbo University (NBU20240296). To evaluate the anti-adhesion effect of JGP in the intraperitoneal cavity, a rat cecum adhesion model was used.SD rats (male, 8 weeks, 220 g–250 g) were anesthetized by intraperitoneal injection of sodium pentobarbital. The skin was incised in the left lower abdomen, and the cecum was gently exposed, and then the cecum was rubbed repeatedly with sterile gauze on the cecum until the surface of the cecum showed obvious bleeding spots. JGP was then applied over the damaged cecum, and the control group was left untreated. Penicillin was given postoperatively to prevent postoperative infection. The rats were executed at 2 weeks postoperatively, the abdominal cavity was opened to observe the adhesions, and the tissues were removed and

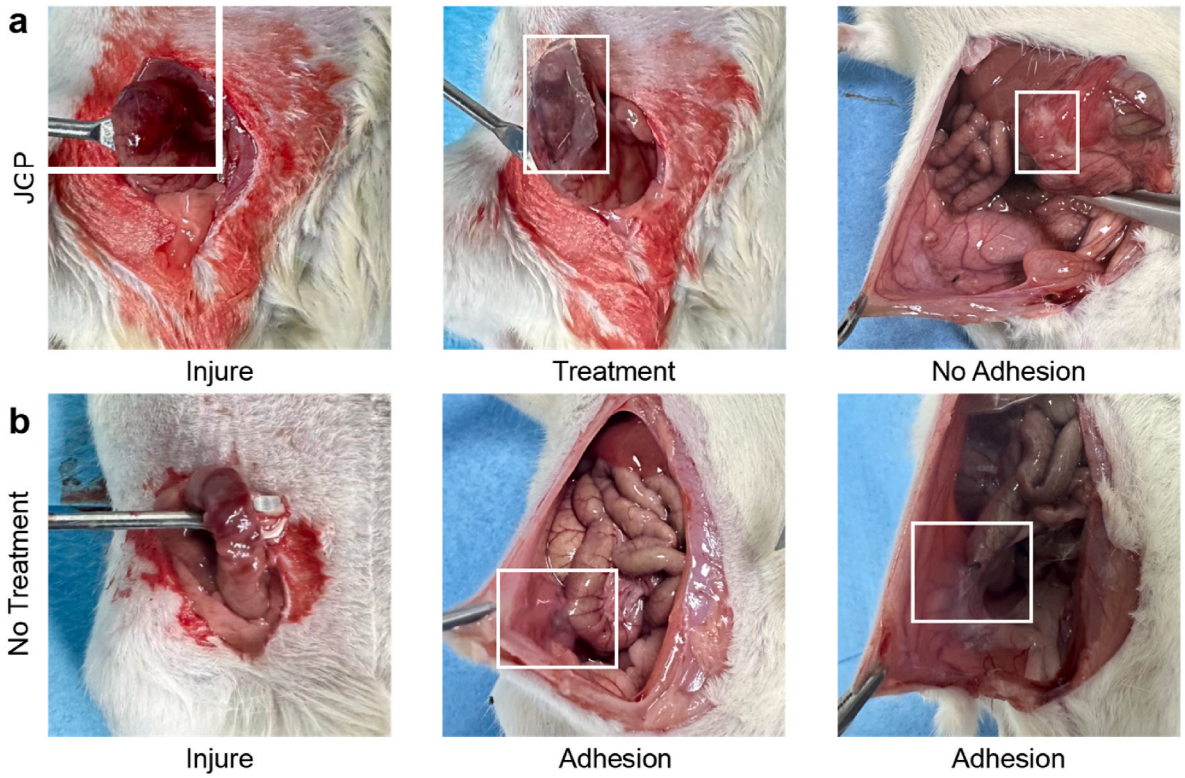

Fig. 8. (a) Experimental procedure and results of abdominal adhesions in the JGP group. (b) Experimental procedure and results of abdominal adhesions in the untreated group.

subjected to HE staining and Masson staining.

2.12. Statistical analysis

Comparisons between the two groups were analyzed using paired t-tests. GraphPad Prism software (version 9.5) was used. Results are expressed as mean ± standard deviation (SD), and all experiments were performed at least three times. values of $p < 0.05$ were considered statistically significant and ns were considered not significantly different (* $p < 0.05$, ** $p < 0.01$, *** $p < 0.001$, **** $p < 0.0001$).

3. Results and discussion

3.1. Synthesis of JGP

Asymmetric adhesion/anti-adhesion patches with a bilayer interpenetrating network were prepared in two steps based on a free radical polymerization method. In the first step, AL with adhesion function was prepared by photocrosslinking. Prior to the preparation of AL, THMA and APMA were first polymerized to form p(APMA-co-THMA) with high hydrogen bond density. From ^{1}H NMR analysis, peaks of CH, CH_2 and CH_3 from the polymer backbone were observed at 1.14, 1.58, and 1.87 ppm; peak a from the branched chain of THMA at 3.78 ppm; and peaks b, c, and d from the branched chain of APMA at 3.25, 3.01, and 2.14 ppm (**Fig. S2**). Simultaneous synthesis of GelMA was obtained from ^{1}H NMR analysis and the groups from methacrylic anhydride ($C{=}CH_2$) were observed at 5.64 and 5.40 ppm (**Fig. S3**). After synthesis of the components, AAc, AAc-NHS, p(APMA-co-THMA), GelMA and LAP were mixed by one-pot method and then solidified by UV light to obtain N_XP_Y. The network of AL is referred to as the AAc network. It is mainly composed of AAc and AAc-NHS by photocrosslinking, in addition to the two substances GelMA and p(APMA-co-THMA). For the interior of the network, the AAc network consists of GelMA as a cross-linking point and a dissipative network through the formation of hydrogen bonds between the hydroxyl group on p(APMA-co-THMA) and the carboxyl group of AAc.

In the second step, topologically cross-linked JGP were prepared by immersion and thermal cross-linking. The network of AAL formed by thermal cross-linking is called SBMA network, which is mainly composed of SBMA. SBMA network takes GelMA and MBAA as cross-linking points, and the network is made more solid internally by the electrostatic effect of SBMA. To verify the effective cross-linking of the immersion solution, they were analyzed by SEM and XPS. As shown in Fig. 2a, PSBMA presents a loose and porous structure, while AL presents a smooth and flat structure. The structure changes from a smooth and flat surface to a loose and porous surface as seen in the JGP overlayer. The changes in the chemical composition of the surface before and after SBMA treatment were investigated using XPS. It can be seen from Fig. 2b–e that for the unsoaked surface there are only two peaks at 400.0 eV and 401.5 eV, but for the soaked surface, a new nitrogen (N1s) peak induced by N^+ appears at 402.2 eV. Similarly, two new sulfur (S 2p) peaks caused by $-SO_3^-$ groups appeared on the soaked surface compared to the unsoaked surface. Therefore, it can be determined that SBMA successfully penetrated into the original network and formed an interpenetrating network after cross-linking, which resulted in the formation of the asymmetric two sides of JGP. From the results of SEM and XPS tests, it can be determined that after the formation of the AAc-dominated network, the AL surface was penetrated by SBMA by immersion in SBMA solution. Finally, the SBMA network was formed by thermal cross-linking that interpenetrated with the AAc network. The SBMA network and the AAc network formed a topological entanglement and therefore showed a smooth excess in SEM.

3.2. Tissue adhesive, swelling and sealing properties

Since there are two physiological conditions of dry (e.g., skin surface) and moist (e.g., abdominal cavity) tissue surfaces, this section tested the adhesion performance and sealing properties of AL in both

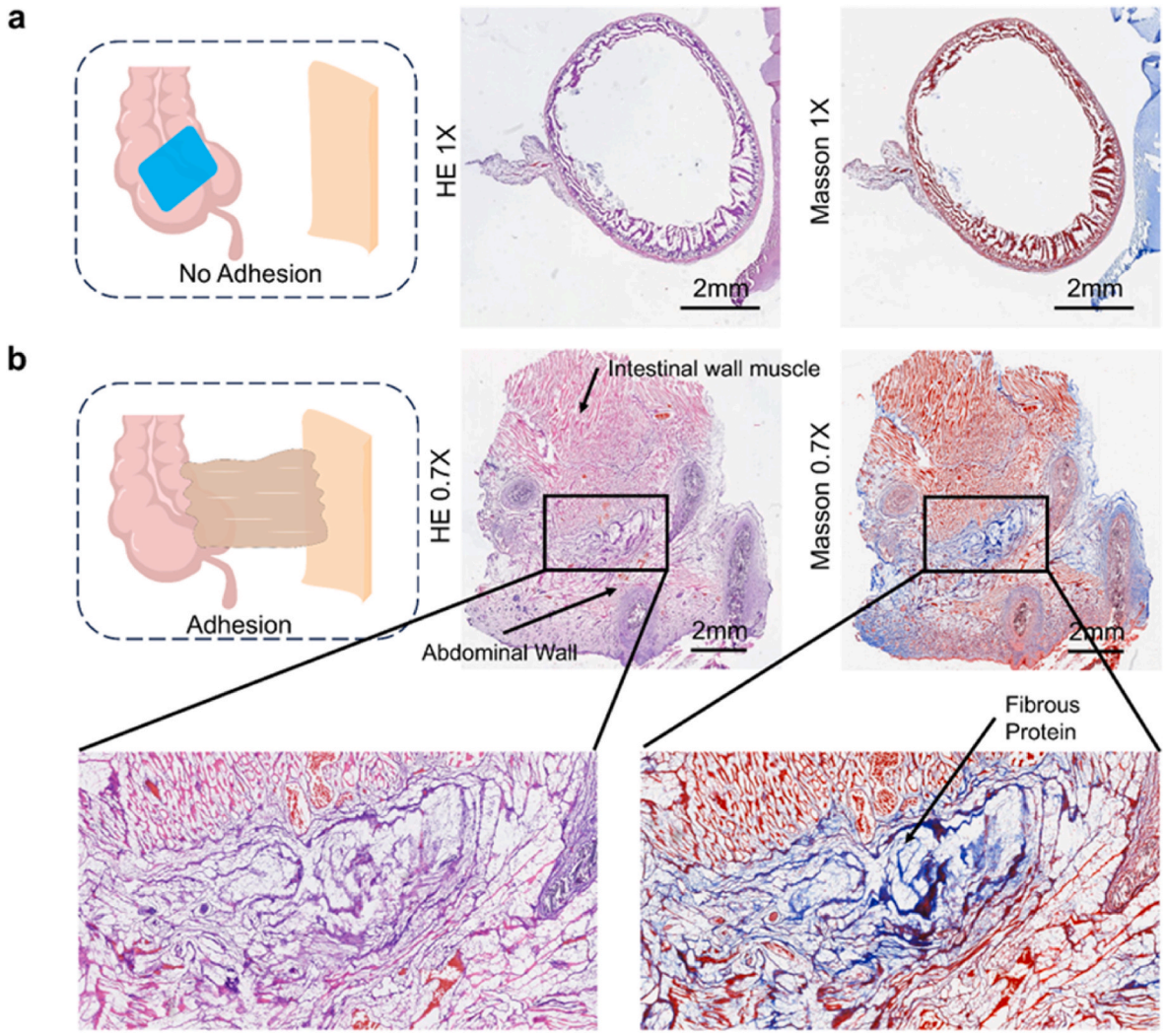

Fig. 9. (a) HE staining of the JGP group. (b) HE staining of the untreated group.

environments. In order to evaluate the adhesion ability of AL to dry tissues, lap-shear experiments were performed on dry pig skin, and the schematic diagram of lap-shear is shown in Fig. 3a. First, the AL was adhered to the dried pig skin and gently pressed for 5 s, and then tested with a soft matter mechanical tester. From the figure, we can see that the adhesion of N_0P_2 without NHS groups is lower than that of N_2P_2, which is mainly due to the fact that NHS can react with the amino groups on the tissue to form amide covalent bonds [31]. When the amount of NHS is certain, the adhesion force exhibits an increasing and then decreasing trend as the content of p(APMA-co-THMA) increases (Fig. 3b and c). The rise is mainly due to the increase in the content of p(APMA-co-THMA) resulting in the formation of more hydrogen bonds between the patch and the tissue. The potential explanations for the observed decline can be proposed. Firstly, an increase in the proportion of p(APMA-co-THMA) may result in enhanced cohesion, as evidenced by the tensile test (Fig. 5a). Secondly, an increase in the proportion of p(APMA-co-THMA) may lead to a depletion of the NHS, due to the ability of the amino group on p(APMA-co-THMA) to form an amide bond with the NHS. Furthermore, an increase in the concentration of p(APMA-co-THMA) results in self-polymerization. AL is capable of forming stable adhesions to a diverse range of materials and organs, including silicone, plastic, glass, metal, heart, liver, and lungs (Fig. 3d).

Strong, fast and long-lasting adhesion is essential for adhesive materials. In particular, the ability to adhere to wet tissues is even more important, primarily because tissues often have blood or tissue fluid outflow due to injury that affects adhesion [36]. Relative to the undried wet gel, the dried dry gel has a better wet tissue adhesion ability, which is due to the fact that the dry gel can remove the hydration layer on the tissue surface by water absorption [31]. To evaluate the wet tissue adhesion ability of AL, the pig skin was first wetted, and then AL was applied to two pieces of pig skin and gently pressed for 10 s, and then tested with a soft matter mechanical tester. By comparing N_XP_Y (undried) and d-N_XP_Y (dried), the wet tissue adhesion performance of d-N_XP_Y was much higher than that of N_XP_Y, which was due to the fact that d-N_XP_Y could remove the hydration layer on the tissue surface. From the lap shear experiment, it can be concluded that the wet tissue adhesion of d-N_XP_Y can reach about 30 kPa, while N_XP_Y can only reach 10 kPa, so the drying method to remove the surface moisture is effective (Fig. 3f and g). In addition to the rapid absorption of surface moisture, d-N_XP_Y also forms adhesion to tissues through multiple hydrogen bonds (from carboxyl and hydroxyl groups) and strong amide covalent bonds. The wet tissue adhesion ability was further confirmed as shown in Fig. 3e and **Video S1**. Pig skin was placed in water, which was adhered by a piece of pigskin with d-N_2P_2 attached, and after 10 s of pressure, d-N_2P_2 was able to hold up a heavy object of about 1.5 kg. Meanwhile, the adhesion performance of the wet tissue was further confirmed by the water current impact experiment. As can be seen in the **Video S2**, d-N_2P_2 can form a stable adhesion with the tissue under the impact of water flow, and it does not fall off under the impact of water flow after adhesion.

Swelling is critical to the performance of wet tissue bonding of hydrogels. On the one hand, wet tissue patches need the ability to rapidly absorb moisture from the tissue surface. On the other hand, the swelling rate of the wet tissue patches cannot be too high because as the patch swells it leads to a decrease in patch adhesion [37]. From Fig. 4a, it can be noticed that all patches reached equilibrium at 5–6 days. Due to the lack of AAc-NHS, the swelling of d-N_0P_2 is much higher than that of the patches of other concentrations, which is unfavorable for durable adhesion. The reason for its large swelling is mainly due to the lack of AAc-NHS, which not only reduces the network cohesion but also weakens the hydrophobicity. In addition, the swelling rate at equilibrium for all four groups, d-N_2P_2 to d-N_2P_5, is 70%–80 %, which is favorable for durable adhesion. As p(APMA-co-THMA) increased from 2 % to 5 %, the swelling rate at equilibrium did not decrease sequentially, which may be due to the hydrophilicity of the hydroxyl group and cohesion interaction. It is noteworthy that there is a significant difference between the swelling rates of d-N_2P_2 and JGP. JGP has a much lower swelling rate, which contributes to long-lasting adhesion (Fig. 4b). The reason for this phenomenon is mainly due to the more stable structure of the bilayer network. It is worth noting that the dissolution of JGP and d-N_2P_2 behaved similarly and did not bend, as shown in **Fig. S4**. Therefore, we consider the immersion of SBMA to be reasonable. In order to determine the solubility at different pH conditions, we tested at pH 2 and pH 10. The swelling increased significantly in both strong acid and base environments. For the strong acid environment, the possible reason for the increase in swelling is the conversion of -NH_2 to -NH_3^+ and the significant increase in hydrophilicity. For the strong base environment, the possible reason for the significant increase in swelling is the conversion of -COOH to -COO^-, which increases the hydrophilicity (Fig. 4b). To evaluate the effect of swelling on the adhesion properties, d-N_XP_Y with bonded pig skin was placed in PBS and subjected to lap-shear experiments for 1, 2, 3, 4, and 5 days at a temperature of 37 °C and 60 rpm with shaking. When reaching the 5th day of dissolution equilibrium, the adhesion force was still about 20 kPa, which indicates that AL has a long-lasting adhesion property. This is mainly due to the role of strong amide covalent and hydrogen bonds, especially the triple-dentate hydrogen bond in p(APMA-co-THMA), which is essential for long-lasting adhesion [30]. Due to the synergistic effect of the triple-dentate hydrogen bond, the loss of the hydrogen bond can be slowed down and the lifetime of the hydrogen bond can be prolonged [38].

In addition, sealing tests on isolated porcine organs (stomach, heart, and lungs) were explored to investigate wet tissue adhesion capabilities and sealing performance. As shown in Fig. 4d and e and **Video S3**, JGP could achieve a rapid seal on a water-filled porcine stomach and remain intact after continuous injection of water. Similarly, JGP can achieve a rapid seal on a water-filled pig heart. These are further evidence of good wet tissue adhesion. And we conducted a burst pressure test in order to quantify the sealing. We built our own model, which is shown schematically in **Figs. S6a–d**. As shown in **Fig. S6e** and **Table S2**, the burst pressure can reach 35 kPa. Our hydrogel adhesive has a burst pressure that is significantly higher than normal systolic pressure (120 mmHg) and thus promises to be a good *in vivo* hemostatic sealant.

Also, qualitative tests were performed in order to test the adhesion of PSBMA (AAL) in wet tissues. As shown in **Fig. S7**, AAL has weak adhesion in dry tissues, which may be due to the electrostatic interaction and hydrogen bonding of SBMA with the tissues. Whereas in wet tissues AAL has hardly any adhesion, this is due to the formation of a hydrated layer on the surface of AAL which prevents hydrogen bonding and electrostatic interactions from forming. On the contrary AL has good adhesion in wet environment because of its ability to absorb surface moisture quickly.

3.3. Mechanical properties

Appropriate mechanical properties (tensile and compressive characteristics) are essential for tough and long-lasting adhesion in the abdominal cavity. Considering the complex situation in the abdominal cavity, such as a wet environment, abdominal compression, etc., the undried N_XP_Y and JGP were subjected to tensile test and compression test, respectively. For the tensile test, as shown in Fig. 5a, N_0P_2 can be stretched to more than 15 times of itself due to the lack of AAc-NHS and the small network cohesion, and its Young's modulus is much lower than that of other groups with AAc-NHS. In addition, as the content of p (APMA-co-THMA) increases, the stretchability gradually decreases and the Young's modulus gradually increases (Fig. 5b). It is noteworthy that there is a significant difference in the tensile modulus between JGP and N_2P_2, which is mainly due to the stronger cohesion of the bilayer network. In contrast, JGP and N_2P_2 have similar tensile properties and can stretch to 3–4 times of themselves, which is mainly due to the enhanced dissipative properties of the hydrogel due to the electrostatic effect of SBMA. For the compression test, N_0P_2 exhibits poor compression performance due to the lack of AAc-NHS. In addition, with the increase of p(APMA-co-THMA), the compression performance exhibited similarity to the tensile performance (Fig. 5c). Due to the increase in dissipative properties, there is a gradual increase in stress and a gradual increase in compressive modulus at 80 % strain (Fig. 5d). The JGP is more robust due to the incorporation of the SBMA network and the compressive modulus increases. At 80 % compressive strain, after three compression-unloading cycle tests, both JGP and N_2P_2 can recover to the initial shape (Fig. 5e). And the JGP compression-unloading cycle test stress can reach about 0.7 MPa, which is much higher than the maximum abdominal pressure of the human body (about 0.02 MPa) [39]. The compression and tensile test results show that JGP has multiple physical interactions, excellent energy dissipation and good toughness and recovery, which contribute to durable adhesion in the abdominal cavity.

3.4. In vitro and In vivo biocompatibility and antimicrobial testing

Biocompatibility is crucial for bioadhesives. To assess the in vitro biocompatibility of the patches, extracts of JGP and AL (N_2P_2) were tested separately. In vitro cytotoxicity was first assessed using CCK-8 and live/dead staining. Confocal images showed that L929 cells incubated by JGP- and AL (N_2P_2)-based media showed normal morphology and the trends of cell viability and proliferative behaviors were similar to those of the control group (Fig. 5g). The results of the CCK-8 assay showed that JGP and AL (N_2P_2) were not toxic to the cells from 1 to 3 days (Fig. 5f). The blood compatibility of JGP and AL(N_2P_2) was determined by an in vitro hemolysis assay, which showed that JGP and AL(N_2P_2) did not cause significant hemolysis, with a hemolysis rate of <5 % (Fig. 5h).

To assess the *in vivo* biocompatibility of the patches, subcutaneous degradation experiments were performed on JGP and AL (N_2P_2), which were sampled and observed at weeks 1, 2, 3, and 4, respectively. As can be observed from Fig. 6b, a fibrous capsule had formed on the tissue and encapsulated JGP and AL (N_2P_2) in the first week. During the first two weeks, the volume of the hydrogel swelled due to swelling, and with the metabolism of the organisms, good degradation of both JGP and AL (N_2P_2) had occurred by the fourth week. In HE staining, there were fiber capsules encapsulated at each specific time point, which indicated that JGP and AL (N_2P_2) were well biocompatible. Notably, HE staining showed (Fig. 6c) that AL (N_2P_2) had obvious adhesion to the fibrous tissue, whereas JGP did not have obvious adhesion to the fibrous capsule, which laterally proved the effect of SBMA for anti-cell adhesion. All of the above experiments proved that both JGP and AL (N_2P_2) had good biocompatibility and degradability, indicating that the biocompatibility did not change during the transformation from AL (N_2P_2) to JGP.

In the case of hemorrhage, the wound is susceptible to bacterial infection, so the antimicrobial properties of the patch are critical. For the antimicrobial properties of the patch, the antimicrobial properties of

N_XP_Y and JGP were determined using *Staphylococcus aureus*. From Fig. 7i, it can be seen that there was no significant colony growth around the hydrogel except for N_0P_2, which had good antimicrobial properties. The possible reason for this phenomenon is that AAc-NHS reacts with the bacterial cell wall, whereas N_0P_2 does not have good antimicrobial properties due to the lack of NHS moiety.

3.5. In vivo hemostasis test and anti-abdominal adhesion test

Since JGP exhibits good biocompatibility and good wet tissue adhesion properties, JGP has the potential to be used as a clinical hemostatic material for surgical or accidental bleeding. To evaluate the hemostatic effect of JGP, a liver injury model was used. After exposing the liver, the liver was resected at a certain resection length (Fig. 7b and c). It can be seen in Fig. 7e–g that at 3 min, the untreated heavily bled, the gelatin sponge group bled less, and the JGP group effectively stopped the bleeding. In Fig. 7d, it was shown that the untreated group reached a bleeding volume of nearly 500 mg, the gelatin sponge reached a bleeding volume of about 150 mg, and the JGP only had a bleeding volume of 60 mg. This experiment shows that JGP has good hemostatic effect.

To evaluate the anti-abdominal adhesion effect of JGP, a cecum injury model was used. The abdominal cavity was opened and the cecum was exposed on day 0. The cecum was injured by repeated friction, resulting in the formation of a visible bleeding point in the cecum. The experimental group was divided into a control group (no treatment) and a treatment group (JGP adhesion) (Fig. 7a(ii)). On the 14th day, the abdominal cavity was opened, and it could be observed that the control group already had obvious adhesion bands with fibrin connections between the cecum and the abdominal wall (Fig. 8a). In the treatment group, on the other hand, no adhesion bands were found (Fig. 8b). To quantify the test, we refer to the abdominal adhesion scores from Ito's study, as detailed in **Table S4** [40]. By analysing the results, there was a significant difference between Control group and Treatment, indicating that PSBMA has a good anti-postoperative adhesion effect (**Fig. S8**). As can be obtained by Masson staining, the untreated group had fibrous tissue between the skin and the cecum, whereas the treated group had no visible fibrous tissue due to the action of JGP (Fig. 9a and b). These demonstrated the good anti-abdominal adhesion effect of SBMA.

4. Conclusion

In this study, a Janus hydrogel with wet tissue adhesion and anti-abdominal adhesion properties was designed by drying and one-sided immersion. Its good adhesion, closure, tensile and compression properties were demonstrated by mechano-mechanical property tests. Based on the fast water absorption property of JGP, it exhibits good underwater adhesion properties. It is noteworthy that it can achieve sustained adhesion underwater, which is mainly attributed to the synergistic effect of tridentate hydrogen bonding and the formation of covalent bonds. In addition, both AL and JGP showed good biocompatibility and degradability. In addition, liver injury experiments and cecum injury experiments were performed, and JGP showed good hemostatic effect and anti-adhesion ability. It can be speculated that it may be applied in the field of wound repair because of the good adhesion properties, which provide stable traction for the wound. Its good biocompatibility and antimicrobial properties further provide better conditions for wound repair.

CRediT authorship contribution statement

Hanjie Shao: Writing – original draft, Formal analysis, Data curation, Conceptualization. **Junjie Deng:** Writing – review & editing, Methodology, Investigation, Formal analysis, Data curation. **Zeping Xu:** Writing – original draft, Investigation, Formal analysis, Data curation. **Jiujun Zhu:** Software, Investigation, Data curation. **Wei Jian:** Funding acquisition, Investigation. **Peiru Zhang:** Data curation, Investigation. **Xinhua Zhou:** Project administration, Methodology, Formal analysis. **Xie Zhang:** Investigation, Formal analysis. **Hao She:** Validation, Software. **Jingyun Ma:** Writing – review & editing, Supervision, Methodology, Funding acquisition. **Xiang Wu:** Writing – review & editing, Resources, Investigation, Funding acquisition, Formal analysis, Data curation, Conceptualization. **Hong Li:** Writing – review & editing, Visualization, Supervision, Resources, Methodology, Investigation, Funding acquisition.

Declaration of competing interest

The authors declare that they have no known competing financial interests or personal relationships that could have appeared to influence the work reported in this paper.

Data availability

Data will be made available on request.

Acknowledgements

This study was supported by Ningbo Public Welfare Science and Technology Program (2021S106), Ningbo Major Research and Development Plan Project (No.2024Z215), General Surgery Clinical Key Specialty Construction Project of Zhejiang Province (No.2023-SZZ), Research and Innovation Foundation of Ningbo University (IF2023059), Key Research and Development Program of Ningbo (2022Z132), National Natural Science Foundation of China (12302179), and Zhejiang Provincial Natural Science Foundation of China (Grant No. LTGY24B050001).

Appendix A. Supplementary data

Supplementary data to this article can be found online at https://doi.org/10.1016/j.mtbio.2024.101248.

References

[1] H. An, M. Zhang, Z. Huang, Y. Xu, S. Ji, Z. Gu, P. Zhang, Y. Wen, Hydrophobic cross-linked chains regulate high wet tissue adhesion hydrogel with toughness, anti-hydration for dynamic tissue repair, Adv. Mater. 36 (8) (2024) e2310164, https://doi.org/10.1002/adma.202310164.

[2] R. Mohammadinejad, H. Maleki, E. Larrañeta, A.R. Fajardo, A.B. Nik, A. Shavandi, A. Sheikhi, M. Ghorbanpour, M. Farokhi, P. Govindh, E. Cabane, S. Azizi, A.R. Aref, M. Mozafari, M. Mehrali, S. Thomas, J.F. Mano, Y.K. Mishra, V.K. Thakur, Status and future scope of plant-based green hydrogels in biomedical engineering, Appl. Mater. Today 16 (2019) 213–246, https://doi.org/10.1016/j.apmt.2019.04.010.

[3] M. Su, L. Ruan, X. Dong, S. Tian, W. Lang, M. Wu, Y. Chen, Q. Lv, L. Lei, Current state of knowledge on intelligent-response biological and other macromolecular hydrogels in biomedical engineering: a review, Int. J. Biol. Macromol. 227 (2023) 472–492, https://doi.org/10.1016/j.ijbiomac.2022.12.148.

[4] K. Zhang, X. Chen, Y. Xue, J. Lin, X. Liang, J. Zhang, J. Zhang, G. Chen, C. Cai, J. Liu, Tough hydrogel bioadhesives for sutureless wound sealing, hemostasis and biointerfaces, Adv. Funct. Mater. 32 (15) (2021) 2111465, https://doi.org/10.1002/adfm.202111465.

[5] N.A.N. Hanafy, S. Leporatti, M.A. El-Kemary, Mucoadhesive hydrogel nanoparticles as smart biomedical drug delivery system, Appl. Sci. 9 (5) (2019) 825, https://doi.org/10.3390/app9050825.

[6] A. Shagan, W. Zhang, M. Mehta, S. Levi, D.S. Kohane, B. Mizrahi, Hot glue gun releasing biocompatible tissue adhesive, Adv. Funct. Mater. 30 (18) (2019) 1900998, https://doi.org/10.1002/adfm.201900998.

[7] J. Yu, Y. Qin, Y. Yang, X. Zhao, Z. Zhang, Q. Zhang, Y. Su, Y. Zhang, Y. Cheng, Robust hydrogel adhesives for emergency rescue and gastric perforation repair, Bioact. Mater. 19 (2023) 703–716, https://doi.org/10.1016/j.bioactmat.2022.05.010.

[8] Y. Zhang, C. Li, A. Guo, Y. Yang, Y. Nie, J. Liao, B. Liu, Y. Zhou, L. Li, Z. Chen, W. Zhang, L. Qin, Y. Lai, Black phosphorus boosts wet-tissue adhesion of composite patches by enhancing water absorption and mechanical properties, Nat. Commun. 15 (1) (2024) 1618, https://doi.org/10.1038/s41467-024-46003-6.

[9] X. Wang, Y. Guo, J. Li, M. You, Y. Yu, J. Yang, G. Qin, Q. Chen, Tough wet adhesion of hydrogen-bond-based hydrogel with on-demand debonding and efficient hemostasis, ACS Appl. Mater. Interfaces 14 (31) (2022) 36166–36177, https://doi.org/10.1021/acsami.2c10202.

[10] C. Cui, W. Liu, Recent advances in wet adhesives: adhesion mechanism, design principle and applications, Prog. Polym. Sci. 116 (2021) 101388, https://doi.org/10.1016/j.progpolymsci.2021.101388.
[11] Y. Liang, H. Xu, Q. Han, M. Xu, J. Zhang, J. Wang, X. Liu, Z. Yin, B. Guo, A Janus hydrogel sealant with instant wet adhesion and anti-swelling behavior for gastric perforation repair, Nano Today 54 (2024) 102105, https://doi.org/10.1016/j.nantod.2023.102105.
[12] X. Liu, Y. Yang, H. Yu, L. Wang, Y. Sheng, Z. Huang, J. Yang, Z. Ni, D. Shen, Instant and tough adhesives for rapid gastric perforation and traumatic pneumothorax sealing, Adv Healthc Mater 11 (23) (2022) e2201798, https://doi.org/10.1002/adhm.202201798.
[13] L. Xiong, H. Wang, J. Wang, J. Luo, R. Xie, F. Lu, G. Lan, L.J. Ning, R. Yin, W. Wang, E. Hu, Facilely prepared thirsty granules arouse tough wet adhesion on overmoist wounds for hemostasis and tissue repair, ACS Appl. Mater. Interfaces 15 (42) (2023) 49035–49050, https://doi.org/10.1021/acsami.3c11403.
[14] H. Shao, X. Wu, Y. Xiao, Y. Yang, J. Ma, Y. Zhou, W. Chen, S. Qin, J. Yang, R. Wang, H. Li, Recent research advances on polysaccharide-, peptide-, and protein-bas ed hemostatic materials: A review, Int. J. Biol. Macromol. 261(Pt 1) 129752. https://doi.org/10.1016/j.ijbiomac.2024.129752.
[15] H. Shao, X. Wu, J. Deng, Y. Yang, W. Chen, K. Li, X. Xie, H. She, W. Jian, H. Li, J. Ma, Application and progress of inorganic composites in haemostasis: a review, JMatS 59(17) 7169-7192. https://doi.org/10.1007/s10853-024-09595-4.
[16] K. Chen, C. Liu, J. Huang, L. Che, Y. Yuan, C. Liu, A conformable and tough Janus adhesive patch with limited 1D swelling behavior for internal bioadhesion, Adv. Funct. Mater. 33 (41) (2023) 2303836, https://doi.org/10.1002/adfm.202303836.
[17] A. Narayanan, A. Dhinojwala, A. Joy, Design principles for creating synthetic underwater adhesives, Chem. Soc. Rev. 50 (23) (2021) 13321–13345, https://doi.org/10.1039/d1cs00316j.
[18] W. Wei, L. Petrone, Y. Tan, H. Cai, J.N. Israelachvili, A. Miserez, J.H. Waite, An underwater surface-drying peptide inspired by a mussel adhesive protein, Adv. Funct. Mater. 26 (20) (2016) 3496–3507, https://doi.org/10.1002/adfm.201600210.
[19] E. Kim, J. Jeon, Y. Zhu, E.D. Hoppe, Y.S. Jun, G.M. Genin, F. Zhang, A biosynthetic hybrid spidroin-amyloid-mussel foot protein for underwater adhesion on diverse surfaces, ACS Appl. Mater. Interfaces 13 (41) (2021) 48457–48468, https://doi.org/10.1021/acsami.1c14182.
[20] S.C. Nicklisch, S. Das, N.R. Martinez Rodriguez, J.H. Waite, J.N. Israelachvili, Antioxidant efficacy and adhesion rescue by a recombinant mussel foot protein-6, Biotechnol. Prog. 29 (6) (2013) 1587–1593, https://doi.org/10.1002/btpr.1810.
[21] Y. Zhou, C. Zhang, S. Gao, W. Li, J.J. Kai, Z. Wang, Pressure-sensitive adhesive with enhanced and phototunable underwater adhesion, ACS Appl. Mater. Interfaces 13 (42) (2021) 50451–50460, https://doi.org/10.1021/acsami.1c16146.
[22] M.A. North, C.A. Del Grosso, J.J. Wilker, High strength underwater bonding with polymer mimics of mussel adhesive proteins, ACS Appl. Mater. Interfaces 9 (8) (2017) 7866–7872, https://doi.org/10.1021/acsami.7b00270.
[23] J. Wang, M.H. Suhre, T. Scheibel, A mussel polyphenol oxidase-like protein shows thiol-mediated antioxidant activity, Eur. Polym. J. 113 (2019) 305–312, https://doi.org/10.1016/j.eurpolymj.2019.01.069.
[24] L. Han, X. Lu, K. Liu, K. Wang, L. Fang, L.T. Weng, H. Zhang, Y. Tang, F. Ren, C. Zhao, G. Sun, R. Liang, Z. Li, Mussel-Inspired adhesive and tough hydrogel based on nanoclay confined dopamine polymerization, ACS Nano 11 (3) (2017) 2561–2574, https://doi.org/10.1021/acsnano.6b05318.
[25] K. Li, Z. Xu, X. Liu, Y. He, X. Tian, X. Xu, G. Bo, S. Yuan, L. Xu, M. Yang, J. Yan, H. Zhang, Y. Yan, Mussel foot inspired bionic adhesive material enhanced by a reconstructed in vitro system for interfacial adhesion, Chem. Eng. J. 452 (2023) 139580, https://doi.org/10.1016/j.cej.2022.139580.
[26] W. Zhang, S. Song, J. Huang, Z. Zhang, An injectable, robust double network adhesive hydrogel for efficient, real-time hemostatic sealing, Chem. Eng. J. 476 (2023) 146244, https://doi.org/10.1016/j.cej.2023.146244.
[27] Z. Li, L. Liu, Y. Chen, Dual dynamically crosslinked thermosensitive hydrogel with self-fixing as a postoperative anti-adhesion barrier, Acta Biomater. 110 (2020) 119–128, https://doi.org/10.1016/j.actbio.2020.04.034.
[28] K. Okabayashi, H. Ashrafian, E. Zacharakis, H. Hasegawa, Y. Kitagawa, T. Athanasiou, A. Darzi, Adhesions after abdominal surgery: a systematic review of the incidence, distribution and severity, Surg. Today 44 (3) (2014) 405–420, https://doi.org/10.1007/s00595-013-0591-8.
[29] F.I. Scott, R.K. Vajravelu, R. Mamtani, N. Bianchina, N. Mahmoud, J.K. Hou, Q. Wu, X. Wang, K. Haynes, J.D. Lewis, Association between statin use at the time of intra-abdominal surgery and postoperative adhesion-related complications and small-bowel obstruction, JAMA Netw. Open 4 (2) (2021) e2036315, https://doi.org/10.1001/jamanetworkopen.2020.36315.
[30] L. Sun, J. Zhou, J. Lai, X. Zheng, H. Wang, B. Lu, R. Huang, L.M. Zhang, Novel natural polymer-based hydrogel patches with Janus asymmetric-adhesion for emergency hemostasis and wound healing, Adv. Funct. Mater. (2024) 2401030, https://doi.org/10.1002/adfm.202401030.
[31] H. Yuk, C.E. Varela, C.S. Nabzdyk, X. Mao, R.F. Padera, E.T. Roche, X. Zhao, Dry double-sided tape for adhesion of wet tissues and devices, Nature 575 (7781) (2019) 169–174, https://doi.org/10.1038/s41586-019-1710-5.
[32] X. Wu, J. Deng, W. Jian, Y. Yang, H. Shao, X. Zhou, Y. Xiao, J. Ma, Y. Zhou, R. Wang, H. Li, A bioinspired switchable adhesive patch with adhesion and suction mechanisms for laparoscopic surgeries, Mater Today Bio 27 (2024) 101142, https://doi.org/10.1016/j.mtbio.2024.101142.
[33] M. Yao, H. Sun, Z. Guo, X. Sun, Q. Yu, X. Wu, C. Yu, H. Zhang, F. Yao, J. Li, A starch-based zwitterionic hydrogel coating for blood-contacting devices with durability and bio-functionality, Chem. Eng. J. 421 (2021) 129702, https://doi.org/10.1016/j.cej.2021.129702.
[34] J. Chen, D. Wang, L.-H. Wang, W. Liu, A. Chiu, K. Shariati, Q. Liu, X. Wang, Z. Zhong, J. Webb, R.E. Schwartz, N. Bouklas, M. Ma, An Adhesive Hydrogel with "Load-Sharing" Effect as Tissue Bandages for Drug and Cell Delivery, Advanced materials (Deerfield Beach, Fla.) 32(43) e2001628. https://doi.org/10.1002/adma.202001628.
[35] L. Zhou, L. Zhou, C. Wei, R. Guo, A bioactive dextran-based hydrogel promote the healing of infected wounds via antibacterial and immunomodulatory, Carbohydr. Polym. 291 (2022) 119558, https://doi.org/10.1016/j.carbpol.2022.119558.
[36] W. Peng, C. Liu, Y. Lai, Y. Wang, P. Liu, J. Shen, An adhesive/anti-adhesive Janus tissue patch for efficient closure of bleeding tissue with inhibited postoperative adhesion, Adv. Sci. 10 (21) (2023) e2301427, https://doi.org/10.1002/advs.202301427.
[37] P. Ma, W. Liang, R. Huang, B. Zheng, K. Feng, W. He, Z. Huang, H. Shen, H. Wang, D. Wu, Super-structured wet-adhesive hydrogel with ultralow swelling, ultrahigh burst pressure tolerance, and anti-postoperative adhesion properties for tissue adhesion, Adv. Mater. 36 (11) (2024) e2305400, https://doi.org/10.1002/adma.202305400.
[38] Z.D. Lamberty, N.T. Tran, C.D. van Engers, P. Karnal, D.B. Knorr Jr., J. Frechette, Cooperative tridentate hydrogen-bonding interactions enable strong underwater adhesion, ACS Appl. Mater. Interfaces 15 (29) (2023) 35720–35731, https://doi.org/10.1021/acsami.3c06545.
[39] W. Liang, W. He, R. Huang, Y. Tang, S. Li, B. Zheng, Y. Lin, Y. Lu, H. Wang, D. Wu, Peritoneum-Inspired Janus porous hydrogel with anti-deformation, anti-adhesion, and pro-healing characteristics for abdominal wall defect treatment, Adv. Mater. 34 (15) (2022) e2108992, https://doi.org/10.1002/adma.202108992.
[40] S. Ito, A. Nishiguchi, H. Ichimaru, K. Nagasaka, H. Hirade, T. Taguchi, Prevention of postoperative adhesion with a colloidal gel based on decyl group-modified Alaska pollock gelatin microparticles, Acta Biomater. 149 (2022) 139–149, https://doi.org/10.1016/j.actbio.2022.06.014.